Pergamon

Int. J. Heat Mass Transfer. Vol. 40, No. 2, pp. 311–321, 1997

0017–9310/97 $15.00+0.00

PII: S0017–9310(96)00108–1

Steady-solution selection and existence in geothermal heat pipes—II. The conductive case

MARK J. McGUINNESS

Mathematics Department, Victoria University of Wellington, P.O. Box 600, Wellington, New Zealand

(*Received* 10 *July* 1995 *and in final form* 16 *March* 1996)

Abstract—The behavior of steady geothermal heat pipe solutions is considered, when permeability is reduced to values where conduction effects become important. This extends previous work, in which permeability was large enough for convective effects to dominate. The effect of reduced permeability is studied using computer visualization techniques and qualitative differential equation methods. It is found that as permeability is reduced, conduction effects first appear near a permeability of 10^{-15} m^2, for typical geothermal reservoir parameter values. Solution behavior in the temperature-saturation phase plane is fundamentally affected: solutions starting from pure liquid at cooler temperatures, and having a portion that is gravity-driven and liquid-dominated, can no longer cross to pure vapor at hotter temperatures; and solutions starting from pure vapor at hotter temperatures, and having a portion that is gravity-driven and vapor-dominated, can no longer cross to pure liquid at cooler temperatures. The distinction between vapor-dominated and liquid-dominated solutions disappears, with all solutions having appreciable variations in saturation with depth. Copyright © 1996 Elsevier Science Ltd.

1. INTRODUCTION

This paper is the second of two considering steady heat pipe solutions in the geothermal context. The previous paper [1] considers the case that permeability is large enough to perform a perturbation analysis, and extends previous studies of heat pipe solutions in geothermal reservoirs [2–6]. This second paper considers the case that permeability is reduced to levels such that conduction effects become important, and the perturbation analysis fails. Notation and model follow closely those of Satik *et al.* [2].

In a heat pipe, steam and liquid phases flow in opposite directions, driven by gravity and/or capillary pressure effects, so that heat flows in the direction of steam flow, with little or zero net mass transfer. Recent theoretical and experimental studies of heat pipes include [7–12]. Such a mechanism is important in models of some geothermal reservoirs, as noted in the seminal work of White *et al.* [13]. In the geothermal case there is heating from below, and counterflow is vertical. Steam and heat flow upwards, and liquid flows downwards. Gravity effects have been shown in [1] to dominate over much of the length of the heat pipe when permeability is large, with capillary pressure changes leading to narrow boundary layers that are important in determining which of the two gravity-driven solutions is selected by the boundary conditions.

The present paper considers the effect of reducing permeability to levels where conduction is important, and paves the way for a consideration of the effects of varying permeability in gravity-driven counterflow in geothermal reservoirs. Such considerations are relevant:

(1) in the presence of a cap-rock;
(2) in deeper regions of rapid temperature change such as are seen in the Geysers steam field (e.g. [14, 15]);
(3) in the lower permeability block regions of a double-porosity reservoir; and
(4) near the plastic high-temperature limit at depth in fractured rock.

Purely horizontal heat flow, due to capillary effects, is already well understood, and is not considered here. As noted in [2], there is no loss of generality in taking the model to be vertical, as sketched in Fig. 1, rather than inclined at some general angle to the horizontal.

2. STEADY-STATE COUNTERFLOW

The equations governing steady vertical counterflow, with constant permeability everywhere, and including the effects of conduction and capillary pressure, may be written in the form [1]

$$\frac{\partial P_v}{\partial z} = -\frac{\mathscr{H}(P_v, S)}{\mathscr{F}(P_v, S)} \tag{1}$$

$$\varepsilon \frac{\partial S}{\partial z} = \frac{\mathscr{G}(P_v, S)}{\mathscr{F}(P_v, S)} \tag{2}$$

where the right-hand sides are given in detail in the

NOMENCLATURE

d	unit of permeability [1 darcy = 10^{-12} m^2]
h	specific enthalpy
h_{vl}	latent heat of vaporization
g	gravitational acceleration
J	the Leverett J-function, $1.417(1-s)-2.12(1-s)^2+1.263(1-s)^3$
k	permeability
k_r	relative permeability
md	millidarcy [10^{-3} darcy]
m_l	molecular weight of liquid water [kg kmol^{-1}]
u	mass flux density [kg s^{-1} m^{-2}]
P	pressure
P_c	capillary pressure
Q	energy flux [W m^{-2}]
R	gas constant [m^3 Pa K^{-1} mol^{-1}]
S	liquid saturation
T	temperature [°C]
z	vertical distance [m].

Greek symbols

β	v_l/v_v
ε	perturbation parameter, $(1/P_o)(\partial P_c/\partial S)$
γ	$(T/\mathrm{d}P)(v_v)/(h_{vl}\Delta\rho)$
λ	thermal conductivity
λ_l	liquid mobility, kk_{rl}/v_l
λ_v	vapor mobility, kk_{rv}/v_v
μ	dynamic viscosity
ν	kinematic viscosity
ω	dimensionless heat flow $(Qv_v/(kgh_{vl}\Delta\rho))$
ϕ	porosity
ρ	specific density
σ	surface tension [kg s^{-2}]
$\Delta\rho$	effective density difference $\rho_l - \rho_v(1-(\partial P_c/\partial T)(\partial T/\partial P_v))$.

Subscripts

l	liquid water
v	steam or vapor phase.

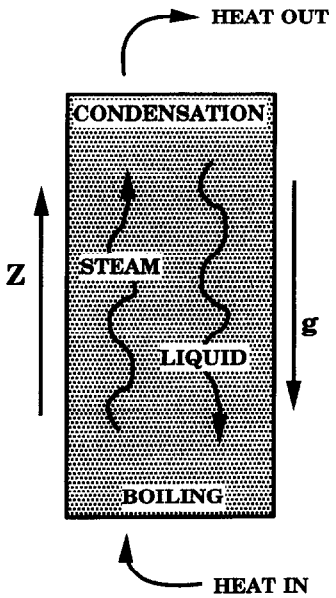

Fig. 1. A sketch of the 1D vertical counterflow model, showing directions of heat and mass flows.

appendix to this paper. Thermodynamic variables have been chosen to be the vapor pressure P_v and liquid saturation S. Occasionally temperature will be used in place of vapor pressure, as they are related for two-phase fluid. Often liquid relative permeability k_{rl} will be used in place of liquid saturation, to keep results independent of the particular choice of relative permeability function.

The parameter ε is proportional to the inverse square root of permeability. It is small when permeability is 10^{-12} m^2, and it increases to one when permeability is reduced to about 10^{-18} m^2.

2.1. *The phase plane*

Solutions to equations (1) and (2) are traditionally plotted as temperature vs depth and saturation vs depth. An alternative is to plot temperature vs saturation, ignoring the depth information, in what is called the phase plane for these two ordinary differential equations.

In the phase plane, one curve denotes a solution with specific values of temperature and saturation somewhere, say at one end of the heat pipe. Many curves represent many possible solutions, each one corresponding to a different choice of boundary conditions. Hence the phase plane is a natural way to view possible solution behaviors, and to see the way that boundary conditions select certain types of solution.

When studying the behavior of solutions as a parameter is varied, the usual approach is to use bifurcation theory. In this approach, the behavior of fixed points in the phase plane is important. These are places where the solution slopes are simultaneously zero, that is, where $\mathscr{H} = \mathscr{G} = 0$. A check of the structure of $\mathscr{H}$ and $\mathscr{G}$ reveals that this can never happen, that there are no fixed points for equations (1) and (2). Then the appropriate structures describing solution behavior, in the absence of the perturbation theory discussed in [1], are the *nullclines*, which are discussed below.

Wherever numerical solutions are plotted in the following, they have been found using the package called STRIDE [17], a Fortran implementation of singly-implicit Runge–Kutta methods for solving stiff and non-stiff ordinary differential equations.

2.2. *Large permeability reviewed*

When permeability is large enough ($k > 10^{-15}$ m^2), ε is less than 0.03, and solutions to these differential equations have narrow capillary boundary-layers. In the boundary layers, saturation changes rapidly, and vapor pressure (or temperature) is almost constant with depth (see Fig. 2).

Provided heat flow values fall within appropriate ranges, the solutions track closely gravity-driven (zero capillarity) outer solutions, over most of the depth range covered, as illustrated in Fig. 2. Thermal conductivity is taken to be 2.0 W m^{-1} °C^{-1}, and linear relative permeabilities and a Leverett J-function formulation for capillary pressure are used for numerical illustrations throughout this paper. The slope of the almost horizontal boundary layers (in the saturation-temperature phase plane) is given by ε. The gravity-driven regions are given by the equation $\mathcal{G} = 0$, which may be plotted in three dimensions ($S, T, Q/k$) to get a hill-shaped surface with a unique local maximum,

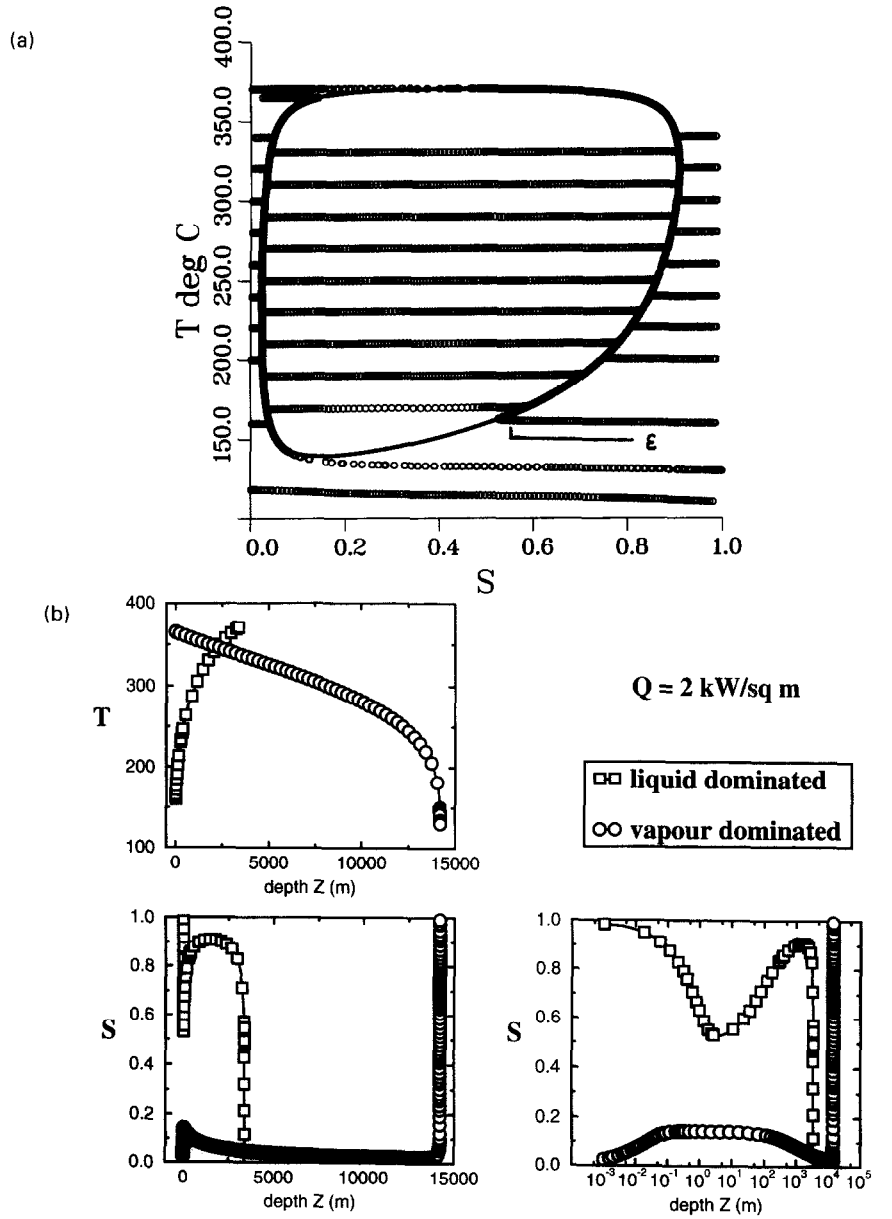

Fig. 2. (a) Solution trajectories (plotted as circles) in the temperature-saturation phase plane, when permeability is 1 darcy, for $Q = 2$ kW m^{-2}. Outer solutions are shown as solid lines. (b) Plots of selected trajectories from (a), showing saturation vs depth and temperature vs depth. Two cases are illustrated, one vapor-dominated, and the other liquid-dominated. One of each of the saturation plots is shown against a log depth scale to show the width of the capillary layers at one end of the trajectories.

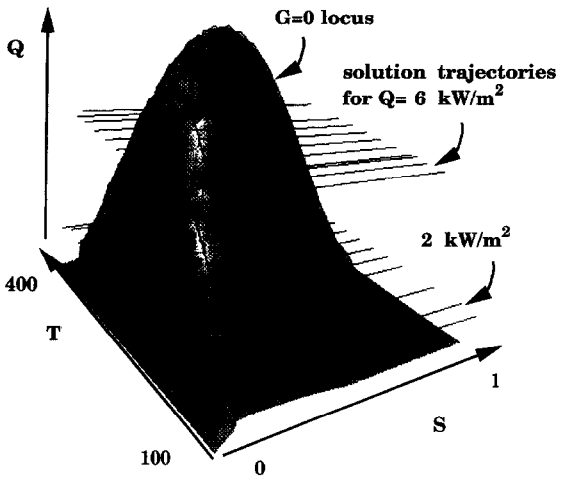

Fig. 3. The $\mathscr{G} = 0$ nullcline surface, for a permeability of 1 darcy, shaded grey and with lines of constant saturation through it, with solution trajectories superimposed for $Q = 6$ kW m^{-2} and $Q = 2$ kW m^{-2}.

whose level contours correspond to the gravity-driven outer solutions. Such a plot is illustrated in Fig. 3. Solutions move on a plane of constant Q/k; when this meets the $\mathscr{G} = 0$ isosurface, gravity-driven solutions exist. When the phase plane lies entirely above or below the $\mathscr{G} = 0$ surface, capillary effects drive the counterflow, and solutions form horizontal lines across the phase plane. In the places where the phase plane is above the $\mathscr{G} = 0$ surface, Udell's [7] criterion of a critical heat flux above which a vapor zone can exist, is satisfied.

The parameter grouping of heat flow divided by permeability is a natural one, as at small epsilon (large k) the shape and height of this $\mathscr{G} = 0$ surface is constant when k is varied (see later, and [1]).

The equation $\mathscr{G} = 0$ may be rearranged to take the form

$$k_{rl}k_{rv} = k_{rl}\left(\omega - \frac{\rho_l\lambda}{k}\gamma\right) + k_{rv}\beta\left(\omega - \frac{\rho_v\lambda}{k}\gamma\right). \quad (3)$$

Using the popular assumption that $k_{rl}+k_{rv} = 1$, a quadratic equation in k_{rl} is obtained:

$$k_{rl}^2 + k_{rl}\left[\omega(1-\beta) + \frac{\lambda\gamma}{k}(\beta\rho_v - \rho_l) - 1\right] + \beta\left(\omega - \frac{\lambda\gamma\rho_v}{k}\right) = 0. \quad (4)$$

The two solutions to this equation (given Q and P_v) are the usual liquid-dominated and vapor-dominated gravity-driven heat pipe solutions, obtained by setting capillary pressure to zero.

The normalized heat flow ω involves the parameter grouping Q/k, and is identical to that used in refs. [2, 7, 8, 10]. However, note that in the present study full temperature dependence of density, enthalpy and viscosity is allowed, so that ω varies with temperature or vapor-pressure. Hence Q/k is used, so that for example fixed values of Q and k (a given heat pipe) lead to solution trajectories lying in a horizontal plane in the computer visualizations. If ω was used as the vertical coordinate, a given heat pipe would have solution trajectories lying on some curved surface in this space, obscuring solution behavior.

3. SMALL PERMEABILITY

Although the boundary layer approach fails for small permeability, it is still useful to consider the curves $\mathscr{G} = 0$. These, and the curves $\mathscr{H} = 0$, form *nullclines* for the differential equations (1) and (2). Nullclines (see for example [18]) are places where solutions move parallel to one of the axes in the phase plane, and a study of nullclines can lead to an understanding of solution behavior, particularly when there are no fixed points as noted above.

There are no $\mathscr{H} = 0$ curves for upwards heat flow at any permeability, reflecting the fact that vapor-pressure or temperature increase monotonically with depth, as expected for a geothermal reservoir. This is clear from a close study of the form of $\mathscr{H}$ (all terms have the same sign), and is confirmed by numerical calculations. Hence solutions to equations (1) and (2) can only move in one direction in the phase plane between any two pressures or temperatures.

The simplest way to see how nullclines change as permeability is reduced is to look at visualizations of the *nullcline surface* $\mathscr{G} = 0$, as in Figs. 4 and 5. These pictures were obtained by numerically evaluating $\mathscr{G}$ for a range of values of temperature, saturation, heat flow and permeability, using accurate fully temperature-dependent thermodynamic variables, and then putting a surface (an isosurface) through zero

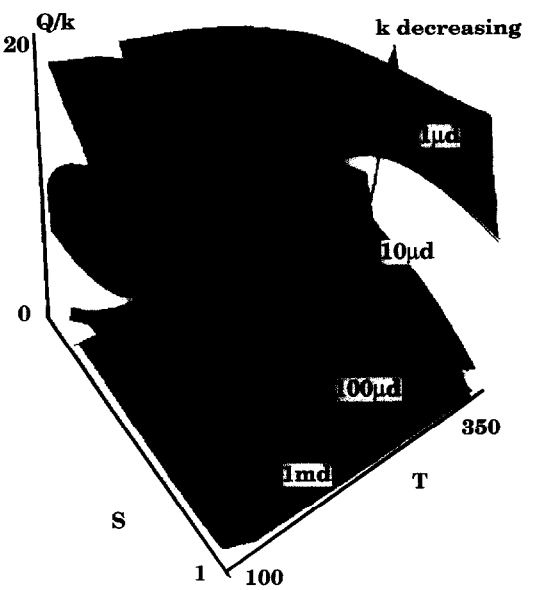

Fig. 4. Nullcline surfaces, for permeabilities 1 d, 100 md, 10 md, 1 md, 100 μd, 10 μd, 1 μd. The vertical (heat flow) coordinate is Q/k in kW d^{-1} m^{-2}.

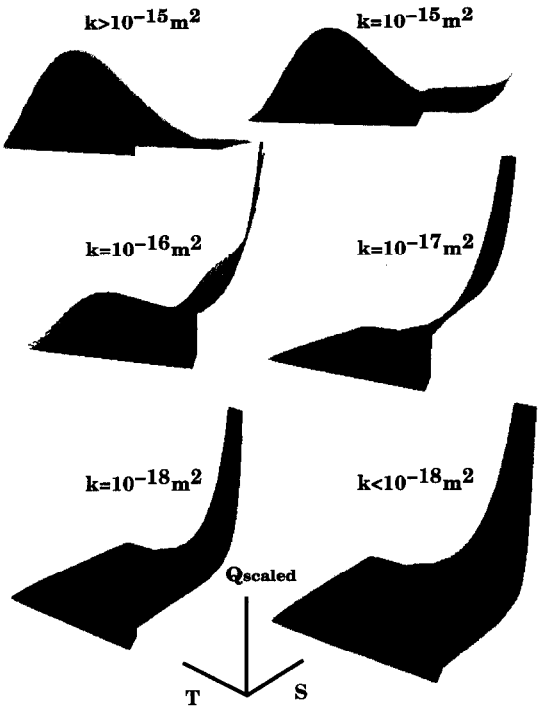

Fig. 5. Nullcline surfaces, for permeabilities varying from 1 darcy to 0.01 μd. The vertical (heat flow) coordinate has been rescaled to reflect the behavior in equation (7), so that $Q/(k\times 10^{16}+1)$ is plotted, with Q in W m^{-2} and k in m^2.

values of $\mathcal{G}$. The calculations were carried out in Fortran on a Silicon Graphics Iris Indigo XS24Z workstation, and the visualisations were performed with Iris Explorer.

For large permeability the appropriate vertical coordinate to use is Q/k. Then the appearance of contours or visualisations of the $\mathcal{G}=0$ surface is unchanging with k. The terminology $\mathcal{G}=0$ *curve* means a level curve (constant Q/k) of this surface.

However, as permeability is reduced below 10^{-15} m^2 the height and shape of the surface changes, and it peels upwards from the corner corresponding to liquid-dominated low-temperature fluid. As permeability is further reduced to values near 10^{-18} m^2, two more significant changes are seen (see Fig. 4):

(1) ε increases, so that solution slopes in boundary layers increase, and the boundary layer approximation fails; and

(2) the height of the $\mathcal{G}=0$ surface increases as the Q/k grouping becomes inappropriate.

These changes are studied numerically and analytically in the following section.

3.1. *Nullcline surface shape changes*

The curves $\mathcal{G}=0$ indicate where solutions can change direction when plotted against saturation. They served as outer solutions in themselves when permeability was large; now they show where the slope of the solution in the temperature-saturation phase plane can change sign.

As noted in [1], as temperature increases towards the critical temperature (about 374°C), all $\mathcal{G}=0$ curves must close (cease to exist), because the latent heat of vaporization tends to zero there.

3.1.1. *Surface height.* Equation (3) rearranges to give

$$\frac{Q}{k}=\frac{k(k_{rl}k_{rv})+(k_{rl}\rho_l+k_{rv}\rho_v\beta)\gamma\lambda}{k\left[ak_{rl}\left(1-\dfrac{\partial P_c}{\partial T}\dfrac{\partial T}{\partial P_v}\right)+\beta ak_{rv}\right]} \tag{5}$$

where

$$a\equiv\frac{v_v}{gh_{vl}\Delta\rho}. \tag{6}$$

The dependence of the right-hand side of equation (5) on permeability has been made explicit. It can be seen that as the permeability k varies, at some fixed pressure and saturation, this equation is of the form

$$\frac{Q}{k}=\frac{kA+B}{k} \tag{7}$$

where A and B are independent of k. In fact, to the nearest power of ten, A varies in size (with S) between zero and approximately 10^{16}, and B is typically about 1. These values are taken at temperatures around 250°C, and are for Q in W m^{-2} and k in m^2.

Note that as temperature approaches the critical temperature where h_{vl} and $\rho_l-\rho_v$ both tend to zero, A tends to zero and B remains close to one in value.

Then for $k\gg 10^{-16}$ m^2, equation (7) becomes

$$\frac{Q}{k}\sim A \tag{8}$$

giving as noted in [1] almost constant Q/k as k varies for large enough permeabilities. This is the case for gravity-driven counterflow.

For $k\ll 10^{-16}$ m^2, equation (7) becomes

$$Q\sim B \tag{9}$$

so that Q itself is almost constant as k varies, for small enough permeabilities.

Equation (9) may be written

$$Q\sim\langle\rho\rangle g\lambda\frac{\partial T}{\partial P_v} \tag{10}$$

where

$$\langle\rho\rangle\equiv\frac{\lambda_l\rho_l+\lambda_v\rho_v}{\lambda_l\left(1-\dfrac{\partial P_c}{\partial T}\dfrac{\partial T}{\partial P_v}\right)+\lambda_v}. \tag{11}$$

That is, since $\langle\rho\rangle$ is a flowing two-phase density (modified by capillary pressure), $\langle\rho\rangle g$ is a pressure gradient, and the right-hand side of equation (10) may be interpreted as a conductive heat flow rate. Hence for small permeability, the nullcline $\mathcal{G}=0$ is a line

along which heat flow is exactly accounted for by conduction.

3.1.2. *Nullcline surface curling.* The quadratic equation (4) for k_{rl} can have two, one or no solutions in the range 0–1 for any given Q, k and T. See Weir *et al.* [16] for a discussion of these solutions when conduction is neglected. For large permeability there is a range of Q and T values for which two solutions in the range 0–1 exist, and distorted circles are obtained for nullclines. These are the gravity-driven outer solutions of [1], and are associated with the hill shape of the $\mathscr{G} = 0$ surface.

For small permeability the effect of conduction is first felt where temperature is lowest. This is because the slope of the Clausius–Clapeyron curve relating temperature and pressure is steepest there, so that temperature gradients are steeper at cooler temperatures. The effective density of two-phase fluid is greater near $S = 1$, so that pressure gradients (and hence temperature gradients) are steeper there. The combination of these is that conductive effects are first seen at the cool liquid-dominated corner of the nullcline surface.

This corresponds to setting the coefficient of k_{rl} in equation (3) to zero,

$$\omega = \frac{\rho_l \lambda}{k} \gamma \tag{12}$$

so that the equation $\mathscr{G} = 0$ then requires that $k_{rv} = 0$. Equation (12) can be solved for temperature, given the values of parameters, to find where the level curve of the nullcline surface meets $S = 1$ in the phase plane. In the same way, the other end of the level curve is given by solving

$$\omega = \frac{\rho_v \lambda}{k} \gamma. \tag{13}$$

Equations (12) and (13) correspond to the extreme values taken by Q in equation (10), conductive heat flow through pure liquid and through pure vapor.

The solution for Q on the $\mathscr{G} = 0$ surface can be shown from equation (10) to be monotonic increasing as k_{rl} increases from zero to one. Hence the surface curls up from the cool liquid-dominated corner and changes smoothly from a hill shape (two solutions for k_{rl}) to a ski slope shape (one solution).

3.2. *An alternative view of nullcline surface changes*

The changes described above may alternatively be viewed using as a vertical coordinate the logarithm of Q. This gives a simpler picture of the changes occurring as permeability is reduced. Visualisations of the nullcline surface with log Q as a vertical coordinate are presented in Fig. 6.

Taking the log of Q is necessary to see the range of heat flow values taken. The surface height reduces like a deflating balloon in these coordinates, as k is reduced, with the edges of the balloon (at $k_{rl} = 0$ and $k_{rv} = 0$) fixed in place. These edges correspond to conductive heat flow, independent of permeability. The center of the surface corresponds to heat flow dominated by gravity-driven convection, when it is above these fixed ends.

It is clear from equation (4) that near $k_{rl} = 0$ or $k_{rv} = 0$, heat flow on the nullcline surface falls to conductive values, no matter the permeability. This puts the previous results for Q/k into perspective; the curling up of the nullcline surface is a consequence of the rescaling on k, with the conductive (fixed) values lying in wait as convective heat flow reduces with k.

3.3. *Solution trajectories in the phase plane*

As permeability is reduced, then, an extra nullcline associated with conductive heat flow appears in the lower right-hand corner of the saturation-temperature phase plane, and moves up the phase plane, gradually dominating the circular nullclines associated with gravity-driven convective heat flow. Figure 7 illustrates this, using numerically calculated values to plot the nullcline curves on the phase plane, reducing permeability while holding the scaled value of Q constant.

The effect this has on solution trajectories in the phase plane is illustrated for a variety of heat flow values, in Figs. 8–10. These have been calculated using the Fortran package called STRIDE [17], an implementation of singly-implicit Runge–Kutta methods designed for both stiff and non-stiff systems of ordinary differential equations. Both figures use linear relative permeabilities and the Leverett J-function approximation for capillary pressure.

Solution trajectories have positive or negative slope depending on whether the $\mathscr{G} = 0$ surface is above or below the plane of constant Q. This follows directly from the differential equations, and from the fact that $\mathscr{H}$ does not change sign for upwards heat flow. A physical interpretation of this is that on the nullclines, heatflow is accounted for without capillary effects, either by gravity-driven convection on the circular curves, or by conduction on the monotonic curves.

When the solution is in a region where the nullcline surface is above the plane of constant Q, there would be too much heat flow in the absence of capillarity. Capillary pressure changes act to drive heat in the direction of increasing liquid saturation. Hence in such a region, solutions move to increase liquid saturation as temperature increases, with capillary-driven heat flow partially opposing the natural direction of heat flow from hotter to cooler temperatures. Hence solution slopes in the phase plane must be positive here.

Similarly, in regions where the nullcline surface is below the constant Q plane, heat flow is augmented by capillary effects, to compensate for the shortfall in heat flow, and solution slopes are negative.

Note that solutions will track a $\mathscr{G} = 0$ nullcline when it is nearly vertical in the T, S phase plane, like parts of the nullclines associated with gravity-driven counterflow. The nullcline associated with conduction is more horizontal, and is not tracked by solutions.

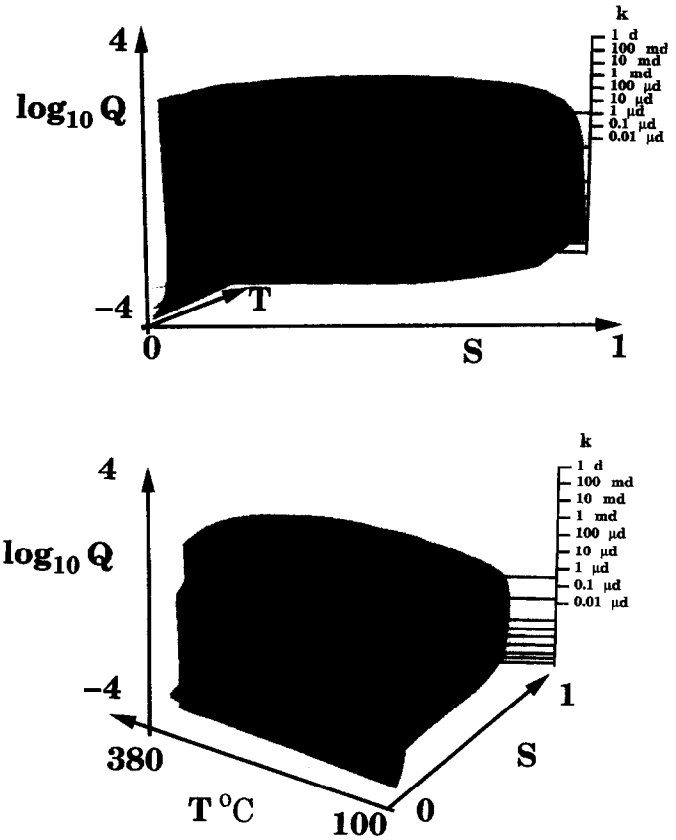

Fig. 6. Nullcline surfaces, for permeabilities varying from 1 darcy to 0.01 μd. The vertical (heat flow) coordinate is log Q, with Q in kW m^{-2}. Two views are shown, from different viewing angles and with varying transparency effects, of the same set of surfaces.

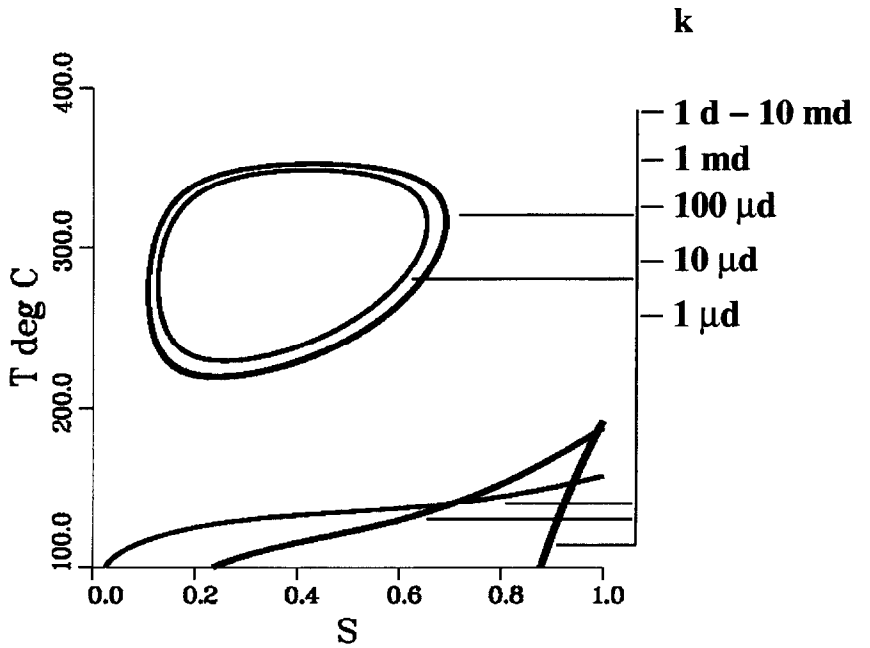

Fig. 7. Nullclines plotted as curves in the phase plane, showing another view of the transition to lower permeabilities, keeping $Q/(k \times 10^{16}+1)$ fixed at 6000 as k varies, with Q in W m^{-2} and k in m^2. Note the appearance of a monotonic curve at the bottom right corner, that moves up to replace the circular curve as permeability is reduced.

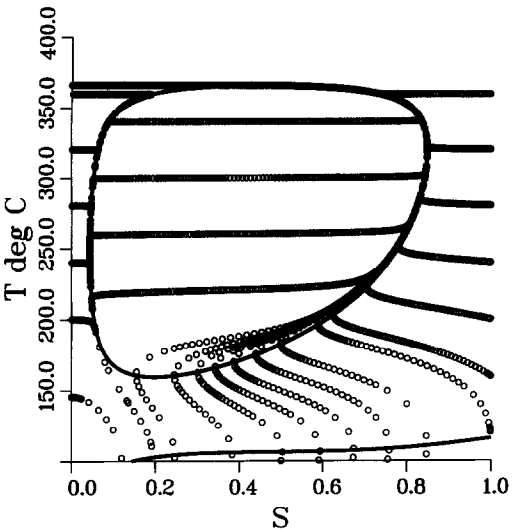

Fig. 8. Solution trajectories in the phase plane, calculated using STRIDE, a Runge–Kutta method. Trajectories (circles) and nullclines (shown as solid curves) are shown, for permeability 1 md and $Q = 3.3$ W m^{-2}.

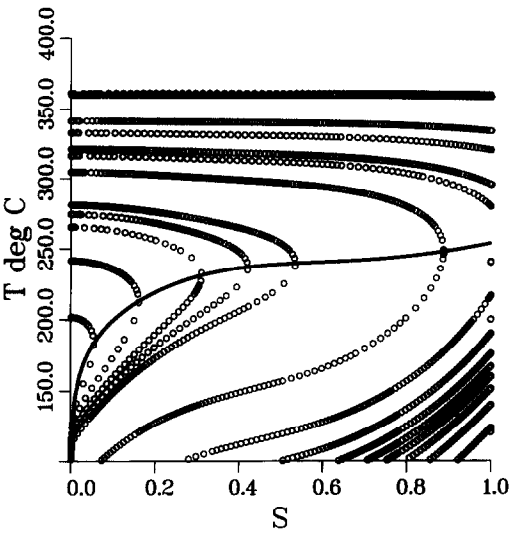

Fig. 10. Solution trajectories in the phase plane, calculated using STRIDE, a Runge–Kutta method. Trajectories (circles) and nullclines (shown as solid curves) are shown, for permeability 10 μd and $Q = 0.22$ W m^{-2}.

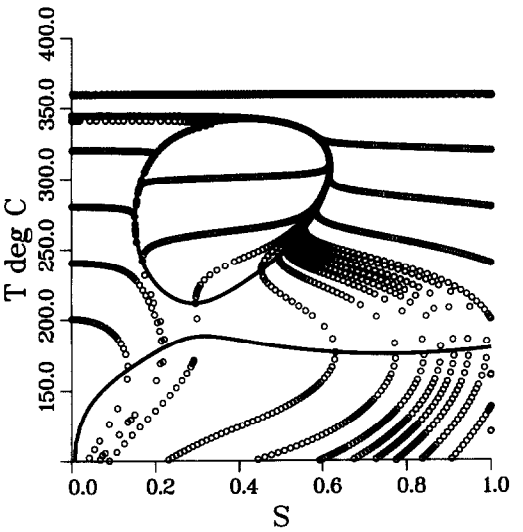

Fig. 9. Solution trajectories in the phase plane, calculated using STRIDE, a Runge–Kutta method. Trajectories (circles) and nullclines (shown as solid curves) are shown, for permeability 100 μd and $Q = 0.76$ W m^{-2}.

Note also in Figs. 8–10 that solution slopes become of order one near the part of the nullcline that is associated with conductive effects. The perturbation expansion employed in [1] becomes invalid when solution slopes are no longer small.

3.3.1. *Crossing to the other side.* An important property of solutions, especially in three-layer models, is whether they cross from one side of the phase plane to the other, connecting between pure liquid and pure vapor phases. The effect of decreasing permeability on this crossing property becomes clear on examining Figs. 8–10. Note that for all cases, if heat flow is high enough, solutions exist that cross from pure liquid at any temperature to pure vapor at a slightly hotter temperature. These are mainly driven by capillary pressure, and do not reach the lengths that gravity-driven solutions attain. The following comments apply to solutions that have a portion in the phase plane that tracks the nullcline, and hence is gravity-driven.

As the nullcline surface lifts up from the cooler pure liquid corner, it introduces a turning point in solutions near there, and prevents there being a solution with negative slope near this corner. This means that as conduction becomes more important (as permeability is further reduced), it is necessary to start a solution at higher and higher temperatures at $S = 1$ [above the temperatures given by equation (12)], if it is to be able to move with negative slope across to the liquid-dominated branch of the nullcline, and eventually at high temperature to pure vapor. What is not obvious from these Figs. 8–10, but is clear from the plots in Fig. 6, is that heat flow must be carefully chosen to decrease along with decreasing permeability, if there is to be any liquid-dominated or vapor-dominated gravity driven branch at all. This is also clear from equation (8). In Fig. 10 these have disappeared altogether, at the low permeability of 10^{-17} m^2. The fact that capillary pressure is driving the counterflow (in concert with conduction) is clear from the differences between vapor and liquid pressures in the trajectory extracted and presented in Fig. 11.

There are some solution trajectories in Fig. 10 that extend from above 300°C down to 100°C. One is shown in Fig. 11. Note that the nullcline meets the solution at about 600 m depth; Fig. 11 shows that above this depth capillary pressure changes slightly oppose conductive heat flow, and below this depth capillary pressure changes act to supplement con-

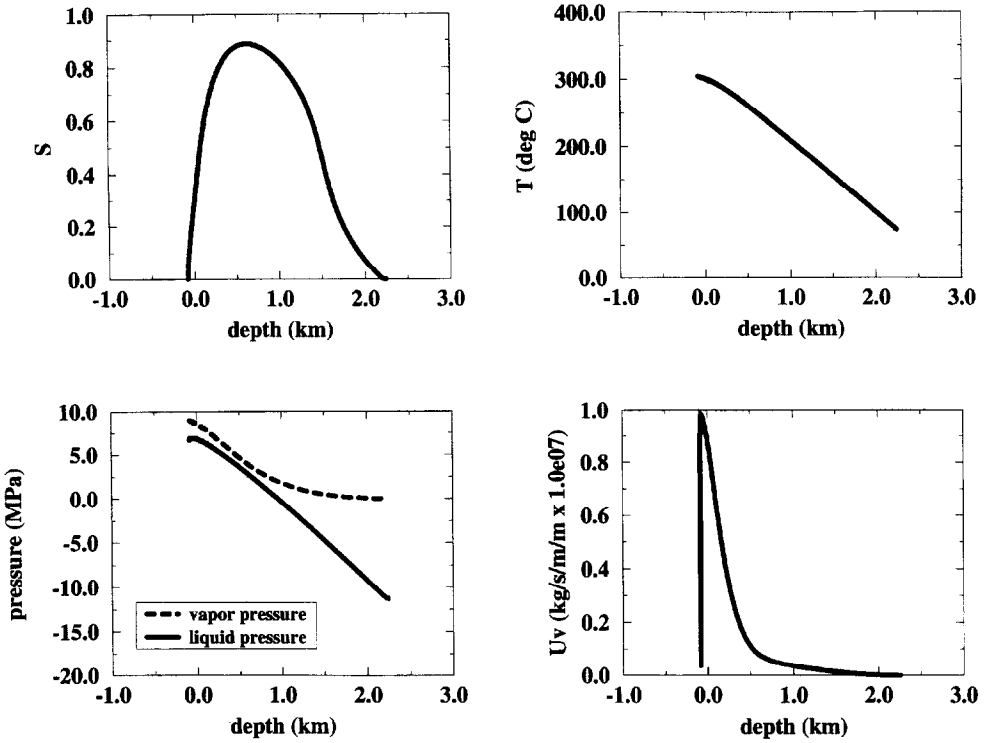

Fig. 11. A particular trajectory extracted from the previous figure, for permeability 10 μd and $Q = 0.22$ W m^{-2}. Saturation, temperature, phase pressures and vapor phase darcy velocity are shown against depth. The zero depth point is arbitrary.

ductive heat flow. Note the almost linear temperature gradient, maintained against the variations in fluid density by varying capillary pressure (visible as the difference between vapor and liquid pressures). Note the absence of saturation boundary layers. There is a boundary layer visible in the velocity of the vapor phase, this has been reported in [2]. On these trajectories, capillary pressure is playing an important part, offsetting imbalances in conductive effects. The role played by gravity has changed from driving counterflow through density differences to simply establishing a pressure gradient (and hence a temperature gradient) through the average two-phase density.

So for small permeability, there are steady heat pipe solutions of large vertical extent, driven by an interplay of capillary and conductive effects, with large variations in saturation over their length.

3.3.2. *Solution selection.* In [1] it was noted that the way trajectories move in the phase plane accounts for the way that choice of boundary conditions selects from either the vapor-dominated or the liquid-dominated gravity driven counterflow solution. As conductive effects become more important in the progression from Fig. 8 to Fig. 10, the distinction between these two solution branches disappears along with the closed $\mathcal{G} = 0$ contours. All solutions have significant variations in saturation over the length of the heat pipe (see Fig. 11), because such saturation variations provide the necessary variations in capillary pressure to balance conduction and give constant heat flux.

3.4. *Heat pipe lengths*

The maximum length of a heat pipe was calculated in [1] by integrating

$$\int_{\mathcal{G}} \frac{1}{g\langle\rho\rangle} \mathrm{d}P$$

along the $\mathcal{G} = 0$ nullcline. As permeability is reduced, the only effect on this calculation is through changes in the nullclines. In particular, the liquid-dominated gravity-driven branch at a given value of Q/k gets pushed off to the right of the phase plane, as the $\mathcal{G} = 0$ surface curls up from the cool corner. This shortens the liquid-dominated branch, and shortens the length of solutions that track it. It also means that steady liquid-dominated heat pipes are restricted to higher temperatures as permeability decreases.

4. CONCLUSIONS

A numerical and analytical study of the transition from convection-dominated to conduction-dominated vertical heat pipes, as permeability is reduced, has been made.

Solutions in the temperature-saturation phase plane move in a way that is controlled by the nullclines of the saturation equation. As permeability is reduced, circular gravity-driven nullclines give way to monoclinic conductive nullclines. Movement of solutions between nullclines is driven by capillary pressure.

Correspondingly, solution slopes between nullclines increase as permeability is reduced, and more solutions in the temperature range 100–350°C correspond to conductive heat flow. Gravity-driven heat flow is characterized by solutions tracking vertical parts of the circular nullcline in the phase plane. Conductive effects are that solutions move with negative slope from high temperatures and low liquid saturations, towards the conductive nullcline, where they reverse slope and head back towards low liquid saturations as temperature continues to decrease.

Acknowledgements—Some subroutines evaluating thermodynamic functions were lifted from the geothermal simulator TOUGH2 [19], and others, extending the valid temperature range up through the critical point, were kindly provided by Warwick Kissling [20]. Visualisations were performed on computer equipment paid for by the New Zealand Lottery Grants Board and by the Internal Grants Committee of Victoria University of Wellington. John Butcher generously provided a copy of STRIDE [17], used to numerically integrate the differential equations.

REFERENCES

1. M. J. McGuinness, Steady-solution selection and existence in geothermal heat pipes—I. The convective case, *Int. J. Heat Mass Transfer* **39**(2), 259–274 (1996).
2. C. Satik, M. Parlar and Y. C. Yortsos, A study of steady-state steam-water counterflow in porous media. *Int. J. Heat Mass Transfer* **34**(7), 1755–1772 (1991).
3. M. J. McGuinness, M. Blakeley, K. Pruess and M. J. O'Sullivan, Geothermal heat pipe stability: solution selection by upstreaming and boundary conditions, *Transp. Porous Media* **11**, 71–100 (1993).
4. M. J. McGuinness, Unstable heat pipes, *Proceedings of the 9th New Zealand Geothermal Workshop*, pp. 147–152. Auckland University, November (1987).
5. M. J. McGuinness, Heat pipe stability and upstream differencing, *Proceedings of the 10th New Zealand Geothermal Workshop*, pp. 117–121. Auckland University, November (1988).
6. M. J. McGuinness, Heat pipe stability in geothermal reservoirs, *Proceedings of the* 1990 *Geothermal Symposium*, GRC, Hawaii, Part I, pp. 1301–1308 (1990).
7. K. S. Udell, Heat transfer in porous media considering phase change and capillary—The heat pipe effect, *Int. J. Heat Mass Transfer* **28**, 485–495 (1985).
8. H. H. Bau and K. E. Torrance, Boiling in low-permeability porous materials, *Int. J. Heat Mass Transfer* **25**, 45–54 (1982).
9. J. P. Sheu, K. E. Torrance and D. L. Turcotte, On the structure of two-phase hydrothermal flows in porous media, *J. Geophys. Res.* **84**(B13), 7524–7532 (1979).
10. G. Schubert and J. M. Straus, Steam-water counterflow in porous media, *J. Geophys. Res.* **84**, 1621–1628 (1979).
11. J. C. Martin, R. E. Wegner and F. J. Kelsey, One-dimensional convective and conductive geothermal heat flow, *Proceedings of the 2nd Workshop on Geothermal Reservoir Engineering*, Stanford University, pp. 251–262 (1976).
12. C. H. Sondergeld and D. L. Turcotte, An experimental study of two-phase convection in a porous medium with applications to geological problems, *J. Geophys. Res.* **82**(14), 2045–2053 (1977).
13. D. E. White, J. P. Muffler and A. H. Truesdell, Vapor-dominated hydrothermal systems compared with hot-water systems, *Econ. Geol.* **66**, 75–97 (1971).
14. G. M. Shook, Vapor pressure lowering in brines and implications for formation of a high temperature reservoir, *Proceedings of the Stanford Geothermal Workshop*, Stanford, California, January (1994).
15. I. Pestov, Mathematical modelling of vapor-dominated geothermal systems, *Proceedings of the 16th New Zealand Geothermal Workshop*, pp. 29–32. Auckland University, November (1994).
16. G. J. Weir and W. M. Kissling, Enhanced conduction in steady, vertical flows of water, steam and carbon dioxide in a porous media, *Transport Porous Media* (submitted).
17. J. C. Butcher, K. Burrage and F. H. Chipman, STRIDE package for differential equations, Mathematics Department, University of Auckland, New Zealand, email chipman@mat.aukuni.ac.nz (1991).
18. W. E. Boyce and R. C. DiPrima, *Elementary Differential Equations and Boundary Value problems*. John Wiley, New York (1992).
19. K. Pruess, SHAFT, MULKOM, TOUGH: a set of numerical simulators for multiphase fluid and heat flow, *Geotermia, Rev. Mex. Geoenergia* **4**(1), 185–202 (1988).
20. W. M. Kissling, Extending MULKOM to supercritical temperatures and pressures, *Proceedings of the* 1995 *World Geothermal Congress*, Vol. 3, pp. 1687–1690, Florence, Italy. IGA, Rome (1995).
21. N. E. Edlefsen, and A. B. C. Anderson, Thermodynamics of soil moisture, *Hilgardia*, **15**(2), 231–298 (1948).
22. R. McKibbin and K. Pruess, Some effects of non-condensible gas in geothermal reservoirs with steam-water counterflow, *Geothermics* **18**(3), 367–375 (1989).

APPENDIX: MATHEMATICAL DETAILS

A steady heat flux is imposed on a two-phase region, with zero net mass flux. Capillary pressure and/or gravity can drive this counterflow.

The flow is one-dimensional and vertical. As noted in [2], the situation with flow inclined at some general (non-zero) angle θ to the horizontal can be transformed to the vertical case by replacing g with $g\sin\theta$. Figure 1 illustrates the conventions for gravity and z directions.

Darcy's law gives the momentum balance for the two phases,

$$u_l = -\frac{kk_{rl}}{\nu_l}\left(\frac{\partial P_l}{\partial z} + \rho_l g\right) \tag{A1}$$

$$u_v = -\frac{kk_{rv}}{\nu_v}\left(\frac{\partial P_v}{\partial z} + \rho_v g\right). \tag{A2}$$

Capillary pressure is taken to be

$$P_c(S,T) = P_v - P_l \tag{A3}$$

and the particular form for P_c is kept general at this point. Vapor-pressure lowering (the Kelvin effect) is also represented in a general way as (after [21])

$$P_v = f_{vpl}(T,S)P_{sat}(T) \tag{A4}$$

where the vapor-pressure lowering factor is approximated by

$$f_{vpl} = \exp\left\{\frac{-m_l P_c(S,T)}{\rho_l R(T+273.15)}\right\} \tag{A5}$$

for illustration purposes, and where P_{sat} is the saturated vapor pressure of bulk liquid, obeying the Clausius–Clapeyron relation

$$\frac{dP_{sat}}{dT} = \frac{\rho_l\rho_v h_{vl}}{(T+273.15)(\rho_l-\rho_v)}. \tag{A6}$$

Mass and energy conservation yield

$$u_l + u_v = 0, \tag{A7}$$

$$u_v h_v + u_l h_l = Q + \lambda \frac{\partial T}{\partial z}. \tag{A8}$$

See also [1, 10, 11, 22] for these. P_v and S are chosen here as the dependent thermodynamic variables. Note that equation (A5) implicitly relates T to P_v and S, and that P_c depends on P_v via T and on S [equation (A3) is taken to define P_l, with P_c a known function of S, T]. These dependencies determine the partial derivatives so that, for example,

$$\frac{dP_c}{dz} = \frac{\partial P_c}{\partial T}\left(\frac{\partial T}{\partial P_v}\frac{\partial P_v}{\partial z} + \frac{\partial T}{\partial S}\frac{\partial S}{\partial z}\right) + \frac{\partial P_c}{\partial S}\frac{\partial S}{\partial z}.$$

Using these dependencies, the conservation equations (A7) and (A8) may be rearranged to obtain

$$\frac{\partial P_v}{\partial z} = -\frac{\mathscr{H}(P_v, S)}{\mathscr{F}(P_v, S)} \tag{A9}$$

$$\varepsilon \frac{\partial S}{\partial z} = \frac{\mathscr{G}(P_v, S)}{\mathscr{F}(P_v, S)} \tag{A10}$$

where

$$\mathscr{F} = \frac{P_0}{H_0}\left[\lambda_l\left(1 - \frac{\partial P_c}{\partial T}\frac{\partial T}{\partial P_v}\right) + \lambda_v\right] \times \left[\lambda_l h_l - \frac{\lambda}{\dfrac{\partial P_c}{\partial S}}\frac{\partial T}{\partial S} + \lambda_l h_l \frac{\dfrac{\partial P_c}{\partial T}\dfrac{\partial T}{\partial S}}{\dfrac{\partial P_c}{\partial S}}\right] \tag{A11}$$

$$-\lambda_l\left[1 + \frac{\dfrac{\partial P_c}{\partial T}\dfrac{\partial T}{\partial S}}{\dfrac{\partial P_c}{\partial S}}\right]\left(\lambda_l h_l + \lambda_v h_v - \lambda_l h_l \frac{\partial P_c}{\partial T}\frac{\partial T}{\partial P_v} + \lambda \frac{\partial T}{\partial P_v}\right) \tag{A12}$$

$$\mathscr{G} = g\left[\left(\lambda_l\left(1 - \frac{\partial P_c}{\partial P_v}\right) + \lambda_v\right)(Q/g + \lambda_l \rho_l h_l + \lambda_v \rho_v h_v)\right. \tag{A13}$$

$$\left. -(\lambda_l \rho_l + \lambda_v \rho_v)\left(\lambda_l h_l\left(1 - \frac{\partial P_c}{\partial P_v}\right) + h_v \lambda_v + \lambda \frac{\partial T}{\partial P_v}\right)\right] \tag{A14}$$

$$\mathscr{H} = -g\left[(Q/g + \lambda_l \rho_l h_l + \lambda_v \rho_v h_v)\lambda_l\left[1 + \frac{\dfrac{\partial P_c}{\partial T}\dfrac{\partial T}{\partial S}}{\dfrac{\partial P_c}{\partial S}}\right]\right. \tag{A15}$$

$$\left. -(\lambda_l \rho_l + \lambda_v \rho_v)\left[\lambda_l h_l\left[1 + \frac{\dfrac{\partial P_c}{\partial T}\dfrac{\partial T}{\partial S}}{\dfrac{\partial P_c}{\partial S}}\right] - \frac{\lambda}{\dfrac{\partial P_c}{\partial S}}\frac{\partial T}{\partial S}\right]\right] \tag{A16}$$

$$\varepsilon = \frac{1}{P_0}\frac{\partial P_c}{\partial S} \tag{A17}$$

and where P_v and z have been non-dimensionalized by dividing by a reference pressure P_0 and a reference depth H_0.